Study of nanoprecipitates in a nickel-based superalloy using small-angle neutron scattering and transmission electron microscopy

E-Wen Huang,[1] Peter K. Liaw,[1] Lionel Porcar,[2] Yun Liu,[2] Yee-Lang Liu,[3] Ji-Jung Kai,[3] and Wei-Ren Chen[4,a)]

[1]*Department of Materials Science and Engineering, The University of Tennessee, Knoxville, Tennessee 37996-2200, USA*

[2]*National Institute of Standards and Technology (NIST) Center for Neutron Research, NIST, Gaithersburg, Maryland 20899-6100, USA*

[3]*Department of Engineering and System Science, National Tsing Hua University, Hsinchu 300, Taiwan, Republic of China*

[4]*Neutron Scattering Science Division, Spallation Neutron Source, Oak Ridge National Laboratory (ORNL), Oak Ridge, Tennessee 37831-6475, USA*

(Received 3 August 2008; accepted 25 September 2008; published online 21 October 2008)

Small-angle neutron scattering (SANS) experiments were performed on a Ni-based nanoprecipitate-strengthened superalloy. A theoretical model for SANS absolute intensity distribution $I(Q)$ was presented to extract the structural properties. During the deformation process, a change in the morphology of precipitates was discovered. However, the average interprecipitate distance and the average volume of precipitates were found to remain invariant. This microstructural information resolved by SANS is in good agreement with the results obtained from the quantitative transmission-electron-microscopy image analysis. © *2008 American Institute of Physics*.
[DOI: 10.1063/1.3002288]

The age-hardening effect, one of the most widely used means for strengthening alloys, was discovered by Wilm.[1] Since then, it has been extensively used for developing various metal-based structural materials for innumerable industrial applications.[2–4] The strengthening mechanism relies on precipitation in some phases other than that of uniform dispersion. The dislocations are localized and prevented from continued movements by the strain field introduced by the lattice mismatch between the precipitates and the homogeneous matrix. The morphology of the precipitates and their spatial arrangement in the embedded matrix are two known key elements in deciding the mechanical performance. Transmission-electron-microscopy (TEM) technique has offered extensive direct observations of local structural characteristics for materials optimization.[5] However due to the finite sampling space, special care is required to extract the ensemble-average information from the taken image. Small-angle neutron scattering (SANS) approach presents a complementary tool to the microscopy technique: it can provide nanoscale information via the measurement of the Fourier transform of the spatial correlation function. However, unlike TEM data, the collected scattering intensity $I(Q)$ is presented in reciprocal Q space and, therefore, to obtain quantitative real-space information, model fitting is usually required. However, in the study of nanoprecipitates, the data analysis is inevitably compounded by the thermodynamically driven polydispersity in the size of precipitates and the anisotropic interprecipitate interference.

The focus of this report is to present a model for SANS $I(Q)$ to facilitate the application of SANS for the study of alloy precipitation strengthening. A recently developed nickel-based alloy[6] with exceptional mechanical performance due to the $Ni_2(Cr,Mo)$ precipitates[7] is selected as an example to demonstrate the applicability of our proposed model. Moreover, a quantitative TEM analysis is used to assess the integrity of the structural information rendered by the SANS experiment.

Our methodology is briefly described as follows. In general, $I(Q)$ obtained from a system consisted of nonspherical particles can be expressed as

$$I(Q) = \frac{N|\Delta\rho|^2}{V_S} P(Q)\{1 + \beta(Q)[S(Q) - 1]\} + I_{\mathrm{INC}}, \tag{1}$$

where $\Delta\rho$ is the difference in scattering-length densities between the particle and the dispersion medium; V_S is the sample volume illuminated by neutron beam; N is the number of precipitates in V_s; $P(Q)$ is the average form factor given by the shape and density profile of particles; $S(Q)$ is the effective one-component interprecipitate structure factor, which is a measure of the interparticle interference; $\beta(Q)$ is the decoupling constant dependent on both the size polydispersity and intraprecipitate density profile,[8] and I_{INC} is the incoherent background.

In the practical implementation of our model fitting, $N|\Delta\rho|^2/V_S$ is treated as a fitting parameter suggested by Pedersen.[9] To minimize the interfacial energy influenced by the strain energy, it is found that $Ni_2(Cr,Mo)$-type precipitates are shaped in the form of polydisperse ellipsoids.[10] Therefore, $P(Q)$ is modeled as

$$P(Q) \equiv P(Q,R) = \int P(Q,x,\delta)N(x,R,\delta)dx \Big/ \int N(x,R,\delta)dx, \tag{2}$$

where

$$P(Q,R,\varepsilon) = \left(\frac{4\pi}{3}R^3\varepsilon^2 \int_0^{\pi/2} \frac{3j_1[Qr(R,\varepsilon,\alpha)]}{Qr(R,\varepsilon,\alpha)} \sin\alpha d\alpha\right)^2 \tag{3}$$

is the form factor of ellipsoids.

a)Electronic mail: chenw@ornl.gov.

$$r(R,\varepsilon,\alpha) = R(\sin^2\alpha + \varepsilon^2\cos^2\alpha)^{1/2}, \quad (4)$$

where R is the long axis, ε is the aspect ratio, and α is the polar angle from 0 to $\pi/2$. The effect of polydispersity is incorporated through the decoupling approximation[8] and a standard Gaussian law[11]

$$N(x,R,\delta) = \frac{1}{\sqrt{2\pi\delta^2}}\exp\left[\frac{-(x-R)^2}{2\delta^2}\right], \quad (5)$$

where δ is chosen to describe the size distribution (δ^2 is the variance).

It is not innovative to apply the scattering techniques to obtain the structural information of colloidal suspensions. The intercolloid structure factor, $S(Q)$ from the Ornstein–Zernike (OZ) integral equation, is in virtue of that colloidal particles are equilibrated through Brownian motions with a suitable closure whose choice is essentially decided by the effective interparticle interaction $V(r)$. This approach has been used previously to provide the structural information of the age-hardened alloys such as Al–Li alloys.[9] However, in our system, the precipitates are formed during a two-step heat treatment initialized by a 16 h annealing at 705 °C and followed by a 32 h cooling at 605 °C.[7] The melting point is found to be 1310 °C.[12] Therefore, the precipitates are generated in a solid-state solution during the heat treatment. Due to the lack of Brownian motion of precipitates, the validity of the OZ-closure approach is, therefore, questionable. To bypass this difficulty, the interprecipitate structure factor $S(Q)$ is calculated via a stochastic phenomenological model. It is assumed that precipitates are partially ordered and separated from the nearest neighbors with a preferred distance, L, with a deviation measured by the root-mean square denoted by σ. The interprecipitate structure factor[13] $S(Q)$ is expressed as a function of Q, L, and σ

$$S(Q,L,\sigma) = 2\left\{\frac{1-\exp[-(Q^2\sigma^2)/4]\cos(QL)}{1-2\exp[-(Q^2\sigma^2)/4]\cos(QL)+\exp[-(Q^2\sigma^2)/2]}\right\} - 1. \quad (6)$$

The incoherent scattering I_{INC} is mainly determined by the measure of $I(Q)$ in a high Q region. Based on a gradient-searching nonlinear least-squares fitting method, the SANS data are analyzed with the inclusion of instrumental resolution. It is important to note that the coherent SANS intensity distributions obtained from the alloy can be fitted uniquely by the current proposed model with five parameters: R, ε, δ, L, and σ. SANS measurements were carried out at the NG-7 SANS instruments in the NIST Center for Neutron Research. The wavelength (λ) of the incident neutrons was selected as 6.0 Å with wavelength spreads $\Delta\lambda/\lambda$ of 15%. The scattering wave vector Q ranges from (0.006–0.32) Å^{-1}. The samples were kept at a constant temperature of (23.0±0.1) °C. For the present SANS-intensity distribution functions placed in an absolute scale, the corrections for detector background and sensitivity have been taken into account.

Figure 1 gives the evolution of true stress as a function of true strain for the alloys before and after heat treatment. Due to the additional strengthening introduced by the presence of the nanoprecipitates interacting with the dislocation activities, at the same strain level, the mechanical property is seen to be enhanced markedly for the aged sample in comparison to the annealed one. For example, the 0.2% yield strength is seen to increase from 376 to 690 MPa.

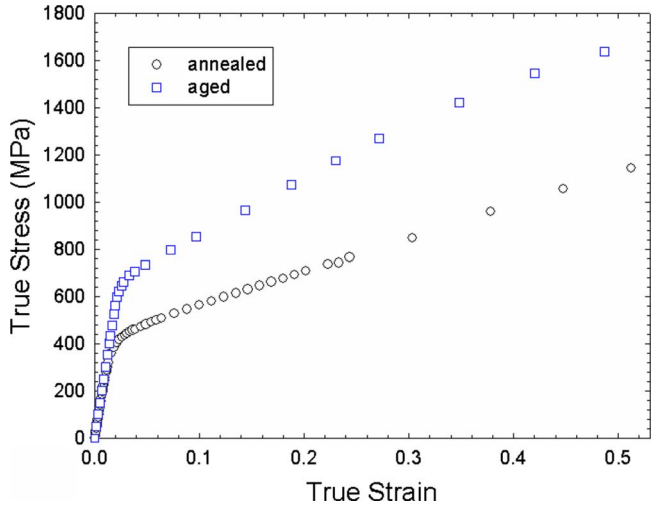

FIG. 1. (Color online) The true stress-strain curves of the annealed (circles) and aged samples (squares). The monotonic-tension experiments were carried out at room temperature with a strain rate of 0.001 /s.

The corresponding SANS data for the alloys (symbols) along with their theoretical fits (curves) incorporating a Q^{-4} contribution at small Q are shown in Fig. 2(a). Unlike bottom two curves, a lack of the interaction peak centered at $Q \approx 0.03$ Å^{-1} for the $I(Q)$ obtained from the annealed sample prior to the aging processes is foremost noticed. Compared with the evolution of the mechanical properties presented in Fig. 1, this observation clearly indicates that the establishment of the interaction peak is due to the precipitates developed during the heat treatment. The bottom two curves with the interaction peak at $Q \approx 0.03$ Å^{-1} were measured from the aged alloy containing the nanoprecipitates. The coherent scattering intensity obtained from the aged alloys is presented in Fig. 2(b). When $Q > 0.03$ Å^{-1}, a clear difference is observed. The quantitative structural information obtained from the SANS-model fitting is given in Table I. It is noticed that within the experimental error, the interprecipitate distance L is seen to remain invariant before and after the deformation. The major structural change resulting

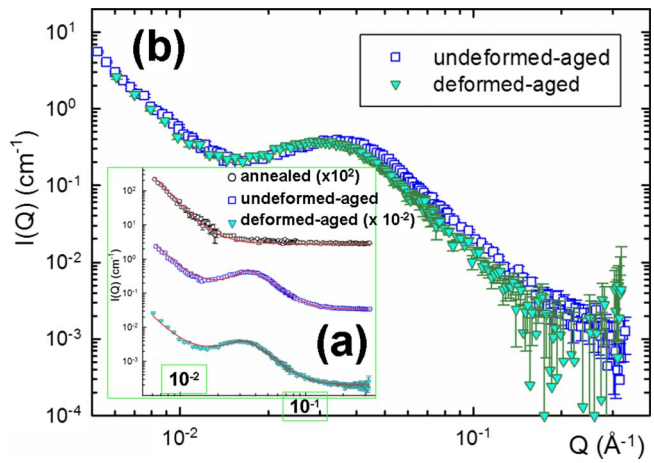

FIG. 2. (Color online) (a) The SANS-intensity distribution obtained from the annealed (circles), the undeformed-aged (squares), the 30%-elongated, deformed-aged samples (triangles), and fits (lines). The curves have been displaced for the sake of better visibility. (b) The coherent scattering obtained from the aged samples: undeformed (squares) and deformed (triangles).

TABLE I. The structural information of the nanoprecipitates (unit: Å).

Aged alloys (containing nanoprecipitates)	Undeformed		Deformed (30% elongation)	
	SANS	TEM	SANS	TEM
Interprecipitate distance (L)	148.3 ± 1.0	158.8	147.1 ± 2.8	135.3
variance of $L(\sigma)$	81.0 ± 0.6	75.8	95.2 ± 1.2	85.9
Radius of the precipitates (R)	57.5 ± 0.5	60.0 (7)	64.1 ± 1.9	64.7
variance of $R(\delta)$	13.1 ± 0.2	50.0 (7)	13.6 ± 0.4	51.2
Aspect ratio of the precipitates (ε)	0.67 ± 0.03	0.64	0.58 ± 0.03	0.50
Volume ($Å^3$)	$(3.57 \pm 0.36) \times 10^5$	3.29×10^5	$(3.70 \pm 0.67) \times 10^5$	3.68×10^5

from the applied stress is the morphological change in the precipitate. After the deformation, the long axis R of the ellipsoidal precipitate is found to increase from 58 to 64 Å while the aspect ratio ε decreases from 0.67 to 0.58. As a result, the average shape of a single precipitate becomes more ellipsoidal. The particle-shearing mechanism,[13] as dislocations cut through the precipitates, increases the variance of the precipitate size. Note that only part of the precipitates located on the shear bands was cut by the dislocations as shown in Fig. 3.

The fact that the applied external stress shows little impact on the average volume of the precipitate (357 ± 35.7 and 370 ± 66.6 nm^3) deserves a special attention. It has been well accepted, as proposed by Eshelby[14] in 1957, that the invariance of the volume of precipitates suggests no exchange of atoms between the precipitates and their embedded matrix during the deformation process. One well-known characteristic of this diffussionless interface is the discrete change in the density when crossing from one phase to another. Based on this picture, it is conjectured that the change in the precipitate morphology is not from the grain growth but due to the spatial rearrangement of the intraprecipitate constituent elements. This hypothesis is not without any physical basis: the aforementioned invariance of L, as shown in Table I, implies that there is no substantial creation or annihilation of precipitates during the deformation process to alter the average distance between the precipitates. Moreover, during the deformation process, a discernable increase in σ, the variance of L from 81 to 95 Å, is also noticed. This observation is believed to be the manifestation of the stress-enhanced shape anisotropy of precipitates as indicated by the increase in the aspect ratio ε. Along with the SANS results, the structural information obtained from TEM analysis is also presented in Table I in a comparative manner. The spatial distribution of the precipitates appearing in the TEM micrograph, such as the example given in Fig. 3(b), is quantitatively identified. The recorded Cartesianized coordinates are further analyzed to resolve the microstructure. As clearly seen from Table I, the results obtained from SANS model fitting are quantitatively consistent with those computed from TEM image analysis. This agreement verifies the applicability of our proposed SANS methodology in exploring the structural properties of nanoprecipitates.

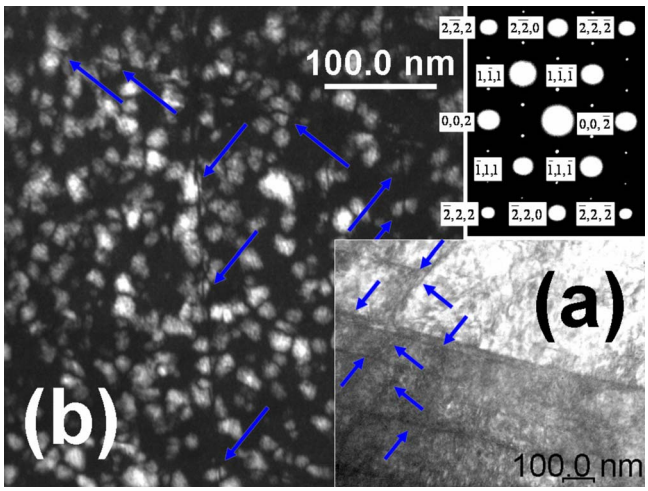

FIG. 3. (Color online) (a) The TEM results of the aged alloy after the 30%-deformation with the [2,2,0]-zone-axis diffraction patterns marked on the top-right. The arrows point the shear bands, which accumulate dislocations. (b) The two-beam-condition TEM showd that only part of the precipitates located on the shear bands is cut.

In conclusion, in this letter we present a SANS $I(Q)$ model combining the $P(Q)$ for polydisperse ellipsoids and a stochastic phenomenological model of $S(Q)$ for studying the structural properties of a nickel-based alloy. Based on our model, a clear deviation in morphology of precipitates is found when a stress is applied. However, the average precipitate volume and interprecipitate distance are seen to remain invariant, suggesting no significant diffusion involved during deformation process. Moreover, the validity of this proposed model is verified and backed by TEM experiments. The major contribution of this letter is that it provides an alternative route for exploring the microstructure of nanoprecipitates embedded in a superalloy in solid state.

International Materials Institutes (IMI) Program (DMR-0231320) National Science Foundation (NSF), supports this research. NIST U.S. DOC provided the neutron-research facilities under the NSF agreement DMR-0454672. We thank Haynes International, Inc.[6] for providing the materials.

[1] A. Wilm, Metallurgie (Halle) **8**, 225 (1911).
[2] E. Hornbogen, J. Light Met. **1**, 127 (2001).
[3] G. B. Olson, Science **277**, 1237 (1997).
[4] M. D. Hollingsworth, Science **295**, 2410 (2002).
[5] H. Gleiter and E. Hornbogen, Mater. Sci. Eng. **2**, 285 (1967).
[6] Certain commercial materials and suppliers identified in this paper do not imply recommendation or endorsement by NIST and ORNL, nor does it imply that the materials are necessarily the best available for the purpose.
[7] Y. L. Lu, L. M. Pike, C. R. Brooks, P. K. Liaw, and D. L. Klarstrom, Scr. Mater. **56**, 121 (2007).
[8] S.-H. Chen, Annu. Rev. Phys. Chem. **37**, 351 (1986).
[9] J. S. Pedersen, Phys. Rev. B **47**, 657 (1993).
[10] M. Kumar and V. K. Vasudevan, Acta Mater. **44**, 1591 (1996).
[11] F. Soisson and G. Martin, Phys. Rev. B **62**, 203 (2000).
[12] A. Arya, G. K. Dey, V. K. Vasudevan, and S. Banerjee, Acta Mater. **50**, 3301 (2002).
[13] R. Giordano, A. Grasso, and J. Teixeira, Phys. Rev. A **43**, 6894 (1991).
[14] G. E. Dieter, *Mechanical Metallurgy*, 3rd ed. (McGraw-Hill, New York, 1986), pp. 73–76.